

A 94-GHz Passive Imaging Receiver using a Balanced LNA with Embedded Dicke Switch

Leland Gilreath¹, Vipul Jain², Hsin-Cheng Yao¹, Le Zheng¹, and Payam Heydari¹

¹University of California, Irvine, CA, 92697 ²SaberTek, Irvine, CA 92614

Abstract — A fully-integrated silicon-based 94-GHz direct-detection imaging receiver with on-chip Dicke switch and baseband circuitry is demonstrated. Fabricated in a 0.18- μm SiGe BiCMOS technology ($f_T/f_{\text{MAX}} = 200$ GHz), the receiver chip achieves a peak imager responsivity of 43 MV/W with a 3-dB bandwidth of 26 GHz. A balanced LNA topology with an embedded Dicke switch provides 30-dB gain and enables a temperature resolution of 0.3-0.4 K. The imager chip consumes 200 mW from a 1.8-V supply.

Index Terms — SiGe, BiCMOS, millimeter-wave, W-band, passive imaging, low-noise amplifiers, power detectors.

I. INTRODUCTION

Passive mm-wave (PMMW) imaging provides the unique capability to create high-resolution images in low-visibility conditions (e.g., through clothing, clouds, and fog) and is therefore useful for such applications as concealed-weapon detection and airplane landing [1]. A low-attenuation atmospheric window from 80-110 GHz (W-band) makes this band an ideal candidate for PMMW systems. The cost of current PMMW cameras is dominated by the W-band compound-semiconductor electronics. Typical III-V-based imaging receivers (RX) are not fully-integrated and require at least two MMW chips [2]. Advanced SiGe BiCMOS technologies with transistor f_T/f_{MAX} beyond 200 GHz can potentially reduce the cost and size of PMMW systems by integrating the MMW RX circuits with imager readout electronics on a single chip.

Passive imagers operate by detecting naturally-emitted thermal (black-body) radiation from an object. Imager performance is measured by the minimum achievable thermal resolution, referred to as the noise-equivalent temperature difference (NETD). NETD depends on the performance of the RX circuits as [2]

$$\text{NETD} = T_{\text{sys}} \sqrt{\frac{1}{BW \cdot \tau} + \left(\frac{\Delta G}{G}\right)^2}, \quad (1)$$

where T_{sys} is the noise temperature at the RX input, BW denotes the MMW bandwidth, τ is the integration time, G is the pre-detection gain, and ΔG is the rms variation of G . A camera frame rate of 25 frames/s limits the maximum integration time to 40 ms, and further reductions in NETD can only be achieved by improvements in the front-end noise figure (NF) and bandwidth. Typical indoor applications such as concealed-weapon detection require an NETD of less than 0.5 K [2].

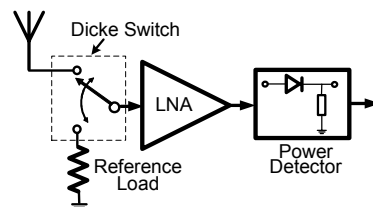


Fig. 1. Conventional direct-detection imaging architecture.

This paper presents the first reported integration of a silicon-based 94-GHz passive imaging receiver with on-chip baseband circuitry. The SiGe BiCMOS RX employs a balanced LNA (using 90° hybrid couplers) and reflection-type binary phase-shifters (RTPS) to realize Dicke-switch functionality with minimal impact of switching loss on NF and NETD performance.

II. RECEIVER ARCHITECTURE

The imaging RX in this work is based on the direct-detection architecture, shown in Fig. 1, as it does not require mixers and complex LO generation associated with a heterodyne detection scheme [3]. In a direct-detection imager, the received MMW radiation is amplified by the LNA and then converted to a DC voltage (proportional to the input power) by the square-law power detector. Since the detector output is a DC voltage, low-frequency phenomena, such as $1/f$ noise and LNA gain fluctuations (ΔG), severely degrade the signal-to-noise ratio at the detector output, and thus become the dominant contributor to NETD. In order to alleviate this problem, an SPDT switch (referred to as a Dicke switch [4]) is typically used to modulate the MMW input signal such that the detector output signal is shifted to a frequency above the $1/f$ noise corner. In the classical architecture of Fig. 1, the SPDT switch is placed directly in front of the LNA and periodically switches the LNA input to either

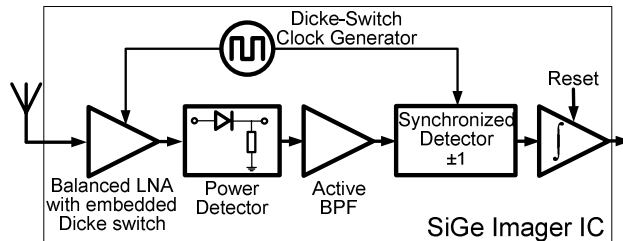


Fig. 2. Block diagram of the proposed SiGe imaging RX.

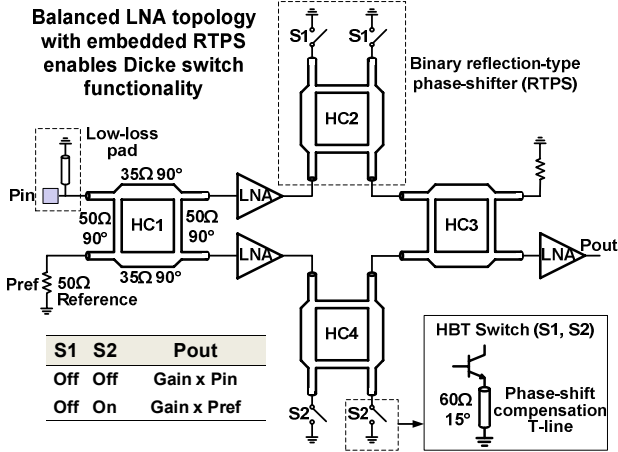


Fig. 3. Balanced LNA with embedded Dicke switch.

the antenna or to a calibrated reference load. By continuously subtracting the two detected signals (antenna and reference), the detector output voltage contributions due to low-frequency fluctuations are canceled (i.e., $\Delta G \rightarrow 0$). The NETD in this case is given by

$$NETD = 2 \cdot T_{sys} / \sqrt{BW \cdot \tau}, \quad (2)$$

where the factor of 2 appears because the Dicke switch is connected to the antenna only for a half cycle. The insertion loss of the switch should be the same in both states, so that the antenna and reference inputs experience the same RF gain. The insertion loss of the switch in Fig. 1 directly adds to the front-end NF, thereby degrading the NETD. Since low-loss switches are available in III-V technologies, this simple architecture has been widely used in practical imagers. On the other hand, silicon-based MMW switches exhibit unacceptably high insertion loss (~5 dB for an HBT switch in our SiGe technology). System-level analysis shows that this 5-dB loss before the LNA will degrade the RX NETD by a factor of 3.

The proposed architecture, shown in Fig. 2, eliminates the above problem by embedding the Dicke switch within a balanced LNA such that it does not degrade the RX noise figure (*cf.* Section III), allowing the system to achieve the lowest possible NETD for a given technology.

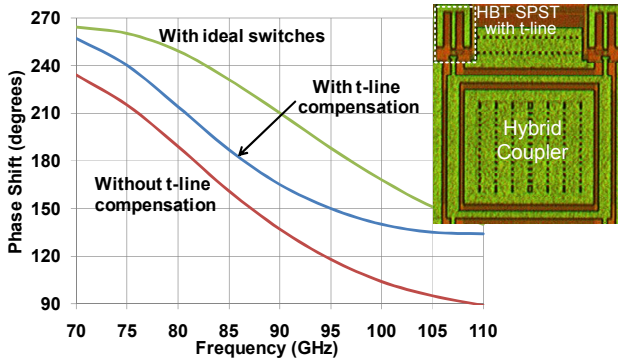


Fig. 4. Simulated RTPS phase shift. T-lines compensate for the HBT SPST.

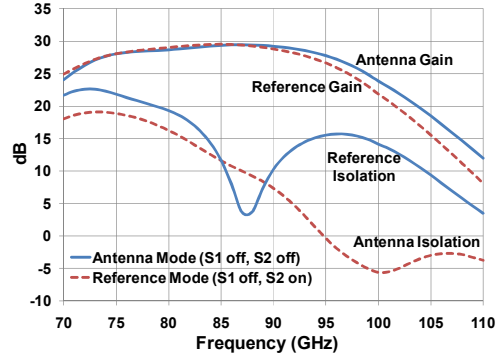


Fig. 5. Measured pre-detection gain and isolation in the two switch states.

The highly non-linear operation of the detector usually results in a high detector NF, necessitating the use of a high-gain LNA (30 dB in this work, *cf.* Section IV).

III. BALANCED LNA WITH EMBEDDED DICKE SWITCH

Fig. 3 shows the schematic of the balanced LNA incorporating the embedded Dicke switch. Inspired by the GaAs topology in [5], the circuit is comprised of a balanced LNA with the addition of a reflection-type binary phase shifter in each branch. When the phase shifters are in the same state (S_1 off, S_2 off), the circuit reduces to a standard balanced LNA, and the amplified signal from the antenna input appears at the output port. However, when the phase shifters are in opposite states (S_1 off, S_2 on), there is an extra 180° phase shift in the reference branch. This results in a constructive amplification of the noise power from the reference input, while the signal from the antenna input is suppressed. By toggling between these two states, the desired chopping operation of the Dicke switch is achieved. System analysis shows that implementing the Dicke switch with this architecture yields a 2x improvement in NETD, as compared with the conventional architecture of Fig. 1.

The switches S_1 and S_2 in the RTPS are implemented using HBTs (Fig. 3). As mentioned in Section II, silicon

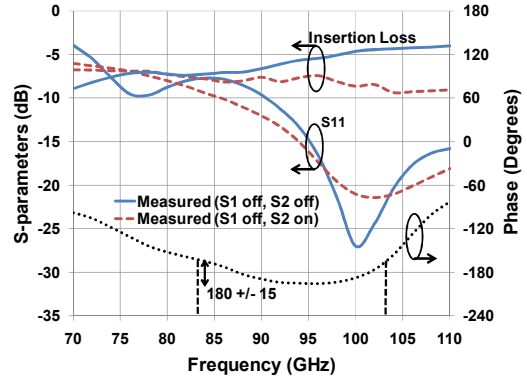


Fig. 6. Measured RTPS S-parameters and output phase difference between the two states.

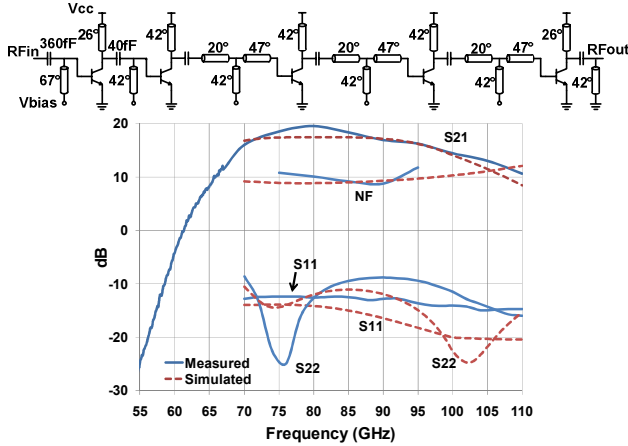


Fig. 7. LNA schematic and its measured performance.

high-speed HBTs make poor switches. Aside from the high insertion loss, they introduce additional phase shift in the on-state, thereby corrupting the phase response of the RTPS. 15° t-line stubs have been used to compensate for the HBT switches and recover the RTPS phase response. As shown in Fig. 4, the t-lines shift the RTPS phase response such that it is closer to that of an ideal switch.

Fig. 5 shows the measured gain and isolation from the antenna and reference ports for the two different phase-shifter states. As expected, in the antenna mode, the signal from the antenna is amplified while the reference signal is suppressed. Similarly, in the reference mode, the reference input is amplified while the antenna signal is suppressed. Note that the balanced structure ensures equal gains in both the antenna and reference modes. An additional LNA is used after the balanced structure in order to achieve a total pre-detection gain of 30 dB. The measured performance of the phase shifter is shown in Fig. 6. The coupler-based RTPS topology provides good input and output return losses over a wide bandwidth.

Each of the three identical LNAs in Fig. 3 is designed as a five-stage amplifier shown in Fig. 7. The HBTs are biased at the optimum-NF current density and exhibit 3.9-dB maximum available gain (MAG) and 7.2-dB NF_{min} at 90 GHz. The theoretical maximum gain and minimum NF of the 5-stage LNA at 90 GHz are 19.5 dB and 9 dB, respectively. The first two stages have been designed for optimum noise match, while the remaining stages are conjugate-matched. In order to minimize matching-network loss, t-lines are implemented as slow-wave coplanar waveguides (CPWs). EM simulations show that a slow-wave CPW achieves 40% higher phase-shift than a conductor-backed CPW for a given length. This translates to 40% reduction in the loss of the matching networks.

The measured LNA gain and NF at 90 GHz are 17 dB and 9 dB respectively (Fig. 7), in good agreement with the calculated predictions. The NF was not measured above

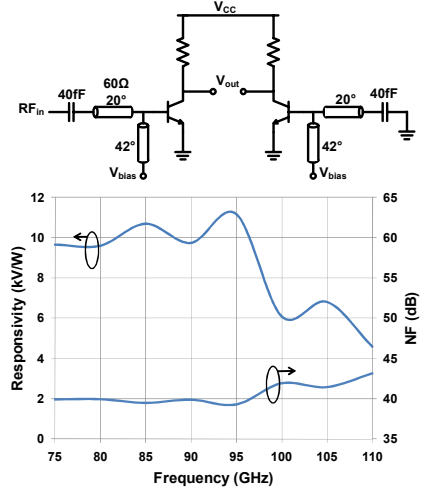


Fig. 8. Detector schematic and its measured responsivity and NF.

95 GHz due to test setup constraints. The LNA draws 35 mA from a 1.8-V supply.

IV. W-BAND DETECTOR

The W-band power detector employs a common-emitter HBT as a square-law device (Fig. 8). The HBT is biased at a low emitter current of $70 \mu\text{A}$ in order to minimize shot noise. A replica common-emitter device is used in order to provide differential outputs to the baseband circuitry. The input matching network provides maximum power transfer and increases the detector responsivity (defined as the ratio of the detector output DC voltage to the input power) by a factor of 3. The detector measurements exhibit a peak responsivity of 12 kV/W and a minimum NF of 39 dB (Fig. 8). The detector NETD is calculated from the measured responsivity and NF as 17 K at 94 GHz. A high-gain LNA is necessary in order to suppress the contribution of the detector NF to the RX NETD. To achieve the target NETD of 0.5 K, 25-to-30-dB pre-detection gain is required.

V. SYSTEM PERFORMANCE

A 4-stage differential ring oscillator generates the 1-MHz Dicke switch clock. Note that, unlike [4], the $1/f$ noise corner in this work is determined by the MOSFETs

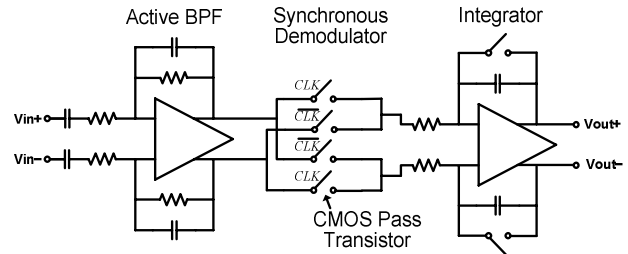


Fig. 9. Simplified schematic of the baseband chain.

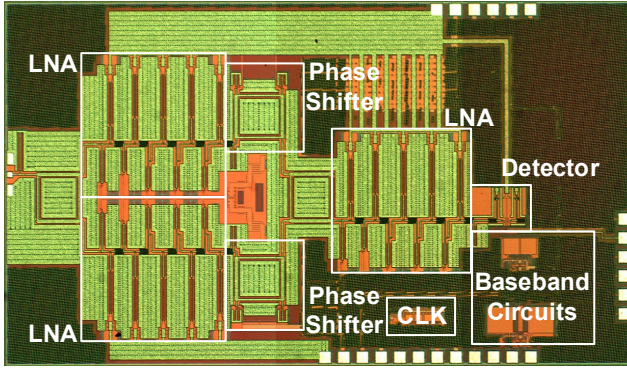


Fig. 10. Die micrograph of the SiGe imaging RX.

(100 kHz) in the baseband circuits. An active bandpass filter (Fig. 9) with an in-band gain of 20 dB and bandwidth of 0.1-10 MHz captures the first 9 harmonics of the detector square-wave output. The synchronous detector and the integrator demodulate the voltage signal, providing a true DC signal at the RX output.

The RX chip has been implemented in a 200-GHz SiGe BiCMOS process offering six metal layers and HBTs with 0.15- μm emitter width. Fig. 10 shows the PMMW RX chip micrograph. The imager chip achieves an NETD of 0.3/0.4 K with integration times of 40/30 ms, meeting the typical specifications for indoor imaging applications. System measurements show a peak responsivity of 43 MV/W and a minimum NF of 12 dB (Fig. 11). The RX draws 110 mA from a 1.8-V supply. Table I summarizes the imaging RX performance, and Table II compares this work with other published W-band imagers. The design in [4] achieves a similar NETD performance using the conventional architecture of Fig. 1. However, it employs a faster 0.12- μm SiGe technology. For comparison, at 90 GHz, the SiGe technology in [4] has a MAG of 6 dB and an NFmin of 5 dB, whereas our technology has a MAG of 3.9 dB and an NFmin of 7.2 dB.

VI. CONCLUSION

A passive mm-wave imaging system operating in the 80-110-GHz atmospheric window has been demonstrated in a 0.18- μm SiGe BiCMOS process. The imager features

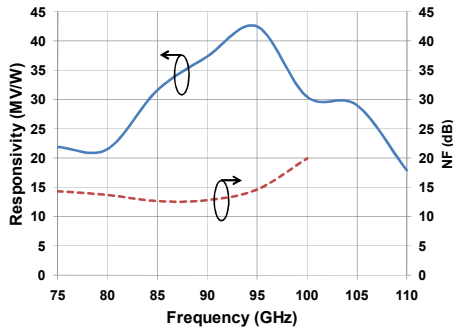


Fig. 11. Measured imager responsivity ($\tau = 30$ ms) and NF.

TABLE I
SUMMARY OF THE RECEIVER PERFORMANCE

Pre-detection Gain	30 dB
3-dB Bandwidth	26 GHz
Noise Figure	12 dB
Responsivity	19–43 MV/W
NETD	0.3/0.4 K ($\tau = 40/30$ ms)
Supply Voltage	1.8 V
Power Dissipation	200 mW
Technology	0.18- μm SiGe BiCMOS ($f_T/f_{\text{max}} = 200$ GHz) MAG = 3.9 dB, NFmin = 7.2 dB @ 90GHz
Die Area	5x2.5 mm ²

TABLE II
PERFORMANCE COMPARISON OF 94-GHZ IMAGERS

Ref.	Technology	Integration	NETD	Responsivity
[3]	InP HEMT	LNA+Detector chipset	0.45 K ¹	0.5 MV/W
[6]	GaAs HEMT	LNA + Detector + Dicke Switch	1.6 K ²	-
[4]	0.13- μm SiGe	LNA+Detector	0.6-0.8 K ³	4 MV/W
[7]	65nm CMOS	LNA + Detector + Dicke Switch	10 K ⁴	0.09 MV/W
This work	0.18-μm SiGe	LNA+Detector+Dicke Switch+Baseband	0.4 K	43 MV/W

¹ $\tau = 3.125$ ms. ² $\tau = 10$ ms. ($\tau = 30$ ms for others)

³Accounting for external Dicke switching. ⁴Calculated from data.

an RTPS-based Dicke switch embedded in a balanced LNA to achieve the lowest possible NETD for a given technology. To the authors' knowledge, the 0.4 K NETD achieved in this work is the lowest reported for a silicon-based imaging RX.

ACKNOWLEDGEMENT

The authors thank Jazz Semiconductor for chip fabrication and Northrop-Grumman Corp. for providing test equipment. This work was supported in part by SRC under contract 2009-VJ-1962.

REFERENCES

- [1] L. Yujiri, M. Shoucri, and P. Moffa, "Passive millimeter-wave imaging," *IEEE Microwave Magazine*, vol. 4, pp. 39-50, Sep. 2003.
- [2] J. J. Lynch, et al., "Passive millimeter-wave imaging module with preamplified zero-bias detection," *IEEE Trans. Microwave Theory Tech.*, vol. 56, no. 7, pp. 1592–1600, July 2008.
- [3] D.C.W. Lo, et al., "A monolithic W-band high gain LNA/Detector for millimeter-wave radiometric imaging applications," *IEEE MTT-S International Symposium*, pp. 1117-1120, June 1995.
- [4] R. H. Dicke, "The measurement of thermal radiation at microwave frequencies," *The Review of Scientific Instruments*, vol. 17, no. 7, pp. 268-275, July 1946.
- [5] J. W. May and G. M. Rebeiz, "High-performance W-Band SiGe RFICs for passive millimeter-wave imaging," *IEEE RFIC Symp.*, pp. 437-440, July 2009.
- [6] D.C.W. Lo, et al., "Novel monolithic millimeter wave multi-functional balanced switching low noise amplifiers," *IEEE Trans. Microwave Theory and Techniques*, Vol. 42, No. 12, pp. 2629-2634, Dec. 1994.
- [7] A. Tomkins, P. Garcia, and S. P. Voinigescu, "A passive W-band imager in 65nm bulk CMOS," *IEEE CSICS*, pp. 1-4, Oct. 2009.